geoconvention
Calgary • Canada • May 15-19 2017

Resolving Ambiguity in AVO and AVAz Inversion

Reza Malehmir, Nasser Kazemi, Douglas R. Schmitt
Experimental Geophysics Group, University of Alberta

Summary

The AVO and AVAz contain valuable information about the elastic properties of a subsurface media. However, the conventional approaches are based on plane-wave theory, which cannot explain observations near the acoustic critical reflection and far offset null reflection at Rayleigh angle. In this contribution, we show our algorithm to understand the acoustic reflectivity of liquid-solid boundary in different incidental and azimuthal directions. This algorithm is a hybrid approach that propagates the wavefield into the space, in frequency domain and reflect each wavenumber with respective reflection coefficient. We used this technique to model the P-wave reflectivity from water-aluminum and water-Phenolic CE interface and then compared it with the observed data against the predicted solution. By accounting for all the interferences and complexities of the reflected wave, this algorithm is able to explain the biases from AVO and AVAz observation inherent in the plane-wave solution.

Introduction

Amplitude variation with offset and azimuth (AVO and AVAz) are well-known examples of this approach in which velocities are calculated using known reflectivity equations [*Aki and Richards*, 1980; *Shuey*, 1985] and many others, are more or less focused in near vertical scattering angles. Figure 1, illustrates a synthetic AVO problem, where the amplitude of the near vertical reflected wave is studied with linearized approaches to the plane-wave reflectivity solution.

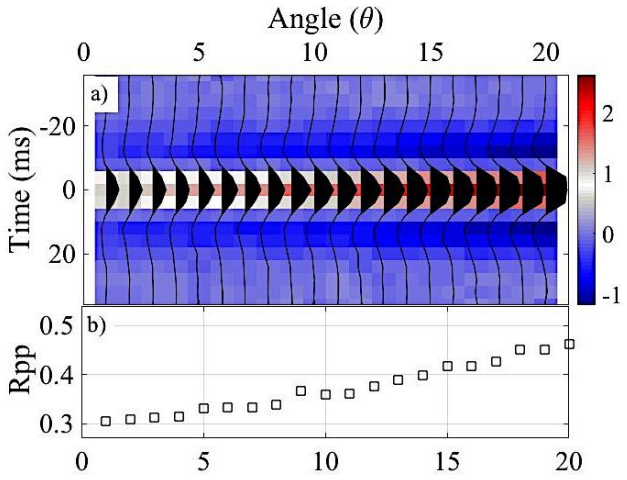

Figure 1 Illustrates a typical AVO a) synthetic seismogram and its b) amplitude variation with angel, which are used in AVO inversion.

There are many assumptions that are used in an AVO problem, that causes an ambiguity to the interpretation. In fact, the incoming elastic wave is considered to be an ideal plane wave which is far from reality and causes artifacts that are reported by many experimentalists [*Alhussain*, 2007; *Bouzidi and Schmitt*, 2008a]. The interpretation of the reflected/transmitted wavefield observed from such a bounded beam requires a proper understanding of how a bounded pulse propagates within elastic media and then scatters at the impedance contrast interfaces. Modeling of the ultrasonic bounded pulse propagation remains challenging, and often simplifying assumptions are used in the analysis of the observations. The usual assumption is that a plane wave of a single wavenumber sufficiently describes the propagation and scattering of a bounded pulse. In reality, a distribution of wavenumbers with differing directions and

frequencies is necessary to capture a bounded pulse; and its behavior can be much more complicated. Such effects include beam diffraction and apparent non-specular reflectivity near the Rayleigh critical incidence angle. Here, we present an algorithm to model bounded planar beam and also study its reflection pattern from a welded boundary in pre and post critical angles. Study of complex reflection and transmission of generated wave-modes at the interface with respect to incident angle could help us in a detailed understanding of the elasticity of the medium.

In this contribution we focus on the complex reflectivity patterns that happens at post-critical angles. At about the Rayleigh angle the amplitude of reflected wave mode decreases significantly which is not predicted by the conventional plane-wave solutions. By complete understanding of this phenomena we might be able to better describe the elasticity of the media, furthermore, this has a potential of skewing the far offset AVO inversion. We believe that this effect is associated with interference of the reflected wave with the incoming wave at the very low incident angle of shear wave critical angle, where surface waves are excited in the lower medium [*Tamir and Bertoni*, 1971]. At the incident angle of the incoming wave where the low amplitude is observed, the reflected wave and surface waves are exactly 180 degrees out of phase, one can calculate the velocity of the surface wave based on the Rayleigh angle and horizontal slowness, [*Bouzidi and Schmitt*, 2000].

Methodology

Modeling of the bounded pulse allows us better predict seismic wave behaviors at the interface, pre- and post- critical angles. First, we show our approach to propagate wave field into the media, then we use it to build our reflectivity model. The bounded beam that is referred in this paper is a frequency limited signal within spatial direction. Take the bounded beam with a dominant frequency of 0.7 MHz and 10cm of width in the x-direction, $\Phi(x;z=0;t)$ is the mathematical representation for the bounded beam at the surface. The first step is to propagate the beam into the elastic media, without losing the generality of the problem, we assume that the beam is traveling from the upper medium and is then reflected from the reflector at the boundary separating two elastic media. So we need an approach to downward continue the bounded beam from the upper half-space and then reflect it from the boundary $z=h$ by upward continuation. Due to mathematical complexities and computational expenses, we chose phase-shift wave equation propagation instead of finite-difference modeling. To propagate the plane-wave into the media, we are using frequency domain phase shift algorithm implemented by [*Bouzidi and Schmitt*, 2008b]. First we look into the wavefield in the frequency domain, in this case, 2D dimensional expression of the source in $\Phi(x;z=0;t)$, equation 1.

$$\Phi(k_x, z=0, \omega) = \frac{1}{4\pi^2} \iint_{-\infty}^{\infty} \varphi(x, z=0, t) e^{(-ik_x x)} e^{(-i\omega t)} \mathrm{dxdt}, \quad (1)$$

where ω and k_x are angular frequency and wave-number in the x-direction, respectively. To propagate the wavefield in the media we are using [*Clearbout*, 1985] phase shift approach, in which the wavefield is downward continued to $z=z_i$, equation 2 describes the phase advance shift in the frequency domain

$$\varphi(\mathrm{x}, \mathrm{z_i}, \mathrm{t}) = \iint_{-\infty}^{\infty} \Phi(k_x, z=0, \omega)\, e^{(-\mathrm{ik_z z_i})}\, \mathrm{e}^{(\mathrm{i\omega t})} e^{(ik_x x)} \mathrm{dk_x d\omega}. \quad (2)$$

Now, it is time to illustrate the geometry of the reflectivity model. Without losing the generality of the problem, let's consider the incoming bounded pulse of in space, hits the boundary at an angle of θ from the normal to the boundary located at the depth of $z=h$. Then, we calculate the reflected wavefield from equation 3 by shifting upward the wavefield from the boundary

$$\varphi(\mathrm{x}, \mathrm{z_i}, \mathrm{t}) = \iint_{-\infty}^{\infty} \Phi(k_x, z=0, \omega)\, e^{(-\mathrm{ik_z h})}\, e^{(\mathrm{ik_z z_i})} \mathrm{e}^{(\mathrm{i\omega t})} e^{(ik_x x)} \mathrm{R}^{\alpha}(\mathrm{k_x}) \mathrm{dk_x d\omega}. \quad (3)$$

where $R(k_x)$ is the complex reflectivity from the boundary for the reflected wave modes α. In this contribution, we focus on the PP reflection where $\alpha=1$. We are calculating R for every k_x from complex Zoeppritz equation in isotropic media or ARTC from [*Malehmir and Schmitt*, 2016] for low symmetric anisotropic media. In order to study the angular variation of reflected amplitude, we should propagate the downgoing wavefield at the respective scattering angle. The reflected amplitude at the surface is recorded for the specular reflection and at the respective position. We have tested this algorithm to predict the laboratory measured reflectivity from water-aluminum (isotropic case) and water-phenolic CE (anisotropic case) and then compared them with the plane-wave solution. For more information about this algorithm and more examples, please refer to [Malehmir et al, 2016].

Examples

To measure the reflectivity from isotropic media, and compare it with a plane-wave solution, and bounded beam modeling, we have chosen cube of aluminum as an isotropic sample to study its reflectivity from its water boundary. The details about the laboratory setup are available in [*Bouzidi and Schmitt*, 2000, 2006, 2008a]. Figure 2 displays the observed acoustic reflected waveform from aluminum, compared with a plane-wave solution and bounded beam amplitude reflectivity along x1 direction and from 12° to 80° incident angles. By looking closely at figure 2b, we observed two major discrepancies between the measured reflectivity data (M_{pp}), the plane-wave solution (P_{pp}) calculated by [*Zoeppritz*, 1919] and the bounded beam (B_{pp}) solution. In all isotropic reflectivities, and around the critical reflection of P-wave (θ_p), we observed that unlike P_{pp}, the R_{pp} is critically reflected with slightly smaller amplitude and at a negligible distance from plane-wave solution. The B_{pp} is able to completely model the observed reflectivity by considering the size of the source and receiver and their associated frequency and wavenumbers, as explained in the previous section. We believe that the interferences from the sides of the source would create a scenario at the θ_p, where some wavenumbers are in pre-critical conditions and others are in critical or post-critical reflection regimes. This interference would create a critical reflection pattern that is smeared in incidental direction and shows smaller amplitude than P_{pp}.

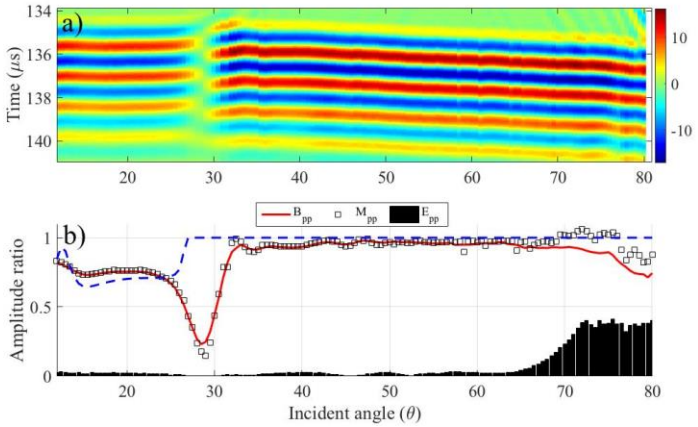

Figure 2.*a) measured reflected waveform from the water-Aluminum boundary, and b) comparison between observed reflectivity (M_{pp}), plane wave solution (P_{pp}) and bounded beam reflectivity (B_{pp}). Percentage error (E_{pp}) is also calculated between M_{pp} and B_{pp}.*

In the anisotropic case, we used the exact laboratory setup and collected reflectivity results from phenolic samples with 0° tilt in four azimuthal directions (ϕ) of 0°, 30°, 60° and 90°. The plane-wave solutions are calculated using anisotropic reflectivity and transmissivity calculator (ARTC) by [*Malehmir and Schmitt*, 2016]. To find the bounded beam reflectivity, we have implemented the acoustic plane-wave solution derived from ARTC along with the geometry of the laboratory setup and the ultrasonic properties of the source. Figure 3a-b displays the measured reflectivity, plane-wave solution and the bounded beam modeling of the reflected wave from 0° tilted Phenolic CE medium in 0° azimuthal direction and incidental angle of 15° to 60°. Figure 2c-d, displays the measured reflectivity (M_{pp}), plane-wave solution (P_{pp}) and the bounded beam modeled reflectivity from the phenolic sample in four azimuthal directions. We can discuss the results in three regimes, I) pre-critical reflection, II) critical reflection and III) post-critical reflection. In pre-critical reflection regime (I), the difference between the observed reflectivity and the plane-wave solution and bounded beam is negligible. We should notice that in the high contrast between water-phenolic boundary, in the pre-critical angle regime, the amplitude variation with incident angle or azimuth is unnoticeable. In the critical acoustic reflection (II), the observed reflection shows smeared reflection with a smaller amplitude than expected in plane-wave solution (P_{pp}). Also, the location of the observed critical angles is happening at a slightly earlier angle than expected in the plane-wave solution. However, bounded beam solution (B_{pp}) is able to predict the observed reflectivity. In the post-critical reflection regime (III), we

observe that the bounded beam is able to predict the data, by including the phase of the reflected beam, included in complex part of the plane-wave reflection coefficients.

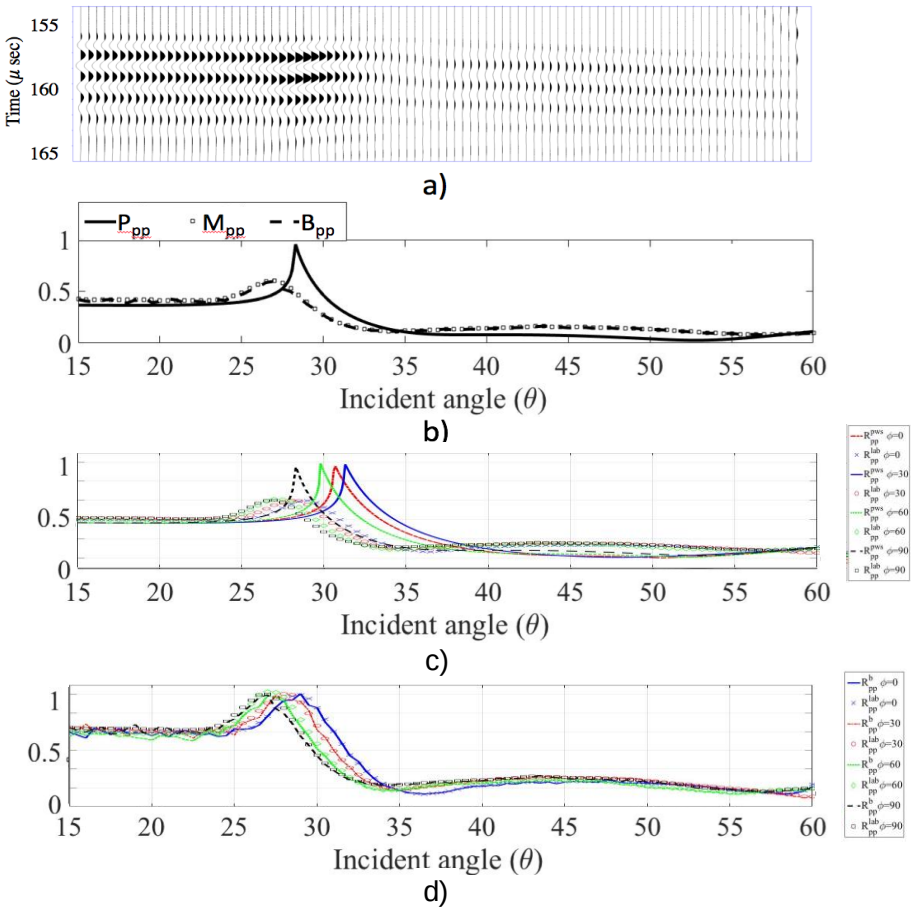

Figure 3*. a) displays the measured reflected ultrasonic waveform from phenolic CE in azimuthal direction ϕ=90°, b) comparison between the observed acoustic reflectivity (M_{pp}), with the plane-wave solution (P_{pp}) and the bounded beam modeled (B_{pp}). c) Displays measured reflectivity in four azimuthal directions against the plane-wave solution and d) bounded beam reflectivity model (line).*

Conclusions

In this contribution, we showcased that the plane-wave solution for wave equation is not enough to predict the acoustic reflectivity from water-solid boundary around the critical reflection and far-offset incidental angles. We provided the algorithm that propagates the observed signal from the source and reflects it from the boundary in the frequency domain. The comparison between the solution from this algorithm and plane-wave solution for acoustic reflection from water- Aluminum boundary expresses that this algorithm was able to recreate the observed acoustic reflectivity. Unlike the conventional plane wave solution, this algorithm is able to model the smooth critical reflection at the observed critical angle. In the far incidental angle, about the Rayleigh angle, this algorithm can successfully model the Schoch shift that is caused by the destructive interference between incoming wave and out-of-phase reflected wavefield. We employed the algorithm to also model acoustic reflectivity from the boundary between water-Phenolic CE block, in which, this algorithm is able to predict the laboratory measured reflection data, in around the P-wave critical angle and Rayleigh null reflection. This algorithm is an essential tool to understand and propagation and reflection of the bounded beam from the isotropic medium.

Acknowledgements

The authors would like to thank NSERC for funding Experimental Geophysics Group (EGG) at University of Alberta.

References

Aki, K., and P. G. Richards (1980), *Quantitative seismology: Theory and methods, v.1*, W.H. Freeman and Co, San Francisco.

Alhussain, M. (2007), Spherical Wave AVO Response of Isotropic and Anisotropic Media : Laboratory Experiment versus Numerical Simulations Mohammed Abdullah K Alhussain, University of Curtin.

Bouzidi, Y., and D. R. Schmitt (2000), Laboratory calibration of amplitude variation with angle using an acoustic goniometer, *70th Ann. Internat. Mtg*, 210–213, doi:10.1190/1.1815863.

Bouzidi, Y., and D. R. Schmitt (2006), A large ultrasonic bounded acoustic pulse transducer for acoustic transmission goniometry: Modeling and calibration, *J. Acoust. Soc. Am.*, *119*(1), 54, doi:10.1121/1.2133683.

Bouzidi, Y., and D. R. Schmitt (2008a), Acoustic reflectivity goniometry of bounded ultrasonic pulses: Experimental verification of numerical models, *J. Appl. Phys.*, *104*(6), doi:10.1063/1.2982094.

Bouzidi, Y., and D. R. Schmitt (2008b), Quantitative modeling of refected ultrasonic bounded beams and a new estimate of the schoch shift, *IEEE Trans. Ultrason. Ferroelectr. Freq. Control*, *55*(12), 2661–2673, doi:10.1109/TUFFC.2008.981.

Clearbout, J. F. (1985), *IMAGING THE EARTH's INTERIOR*, Blackwell Scientific Publications, Oxford, London, Edinburgh, Boston, Palo Alto, Victoria.

Malehmir, R., and D. R. Schmitt (2016), ARTc: Anisotropic reflectivity and transmissivity calculator, *Comput. Geosci.*, *93*, 114–126, doi:10.1016/j.cageo.2016.05.008.

Shuey, R. T. (1985), A simplification of the Zoeppritz equations, *Geophysics*, *50*(4), 609, doi:10.1190/1.1441936.

Tamir, T., and H. L. Bertoni (1971), Lateral Displacement of Optical Beams at Multilayered and Periodic Structures, *J. Opt. Soc. Am.*, *61*(10), 1397–1413, doi:10.1364/JOSA.61.001397.

Zoeppritz, K. (1919), Erdbebenwellen VII. VIIb. Über Reflexion und Durchgang seismischer Wellen durch Unstetigkeitsflächen. Nachrichten von der Königlichen Gesellschaft der Wissenschaften zu Göttingen, *Math. Klasse*, 66–84.